



Disks around Young Planetary-mass Objects: Ultradeep Spitzer Imaging of NGC 1333

Aleks Scholz¹ , Koraljka Muzic^{2,3} , Ray Jayawardhana⁴ , Victor Almen-dros-Abad², and Isaac Wilson⁵¹School of Physics & Astronomy, University of St Andrews, North Haugh, St Andrews KY16 9SS, UK; as110@st-andrews.ac.uk²CENTRA, Faculdade de Ciências, Universidade de Lisboa, Ed. C8, Campo Grande, P-1749-016 Lisboa, Portugal³Faculdade de Engenharia, Universidade do Porto, Rua Dr. Roberto Frias, 4200-465 Porto, Portugal⁴Department of Astronomy, Cornell University, Ithaca, NY 14853, USA⁵Palomar Observatory, California Institute of Technology, Pasadena, CA, USA

Received 2022 December 23; revised 2023 March 17; accepted 2023 March 20; published 2023 April 13

Abstract

We report on a sensitive infrared search for disks around isolated young planetary-mass objects (PMOs) in the NGC 1333 cluster, by stacking 70 Spitzer/IRAC frames at 3.6 and 4.5 μm . Our coadded images go >2.3 mag deeper than single-epoch frames, and cover 50 brown dwarfs, 15 of which have M9 or later spectral types. Spectral types $>M9$ correspond to masses in the giant-planet domain, i.e., near or below the deuterium-burning limit of $0.015 M_{\odot}$. Five of the 12 PMOs show definitive evidence of excess, implying a disk fraction of 42%, albeit with a large statistical uncertainty given the small sample. Comparing with measurements for higher-mass objects, the disk fraction does not decline substantially with decreasing mass in the substellar domain, consistent with previous findings. Thus, free-floating PMOs have the potential to form their own miniature planetary systems. We note that only one of the six lowest-mass objects in NGC 1333, with spectral type L0 or later, has a confirmed disk. Reviewing the literature, we find that the lowest-mass free-floating objects with firm disk detections have masses $\sim 0.01 M_{\odot}$ (or $\sim 10 M_{\text{Jup}}$). It is not clear yet whether even lower-mass objects harbor disks. If not, it may indicate that $\sim 10 M_{\text{Jup}}$ is the lower-mass limit for objects that form like stars. Our disk-detection experiment on deep Spitzer images paves the way for studies with JWST at longer wavelengths and higher sensitivity, which will further explore disk prevalence and formation of free-floating PMOs.

Unified Astronomy Thesaurus concepts: [Brown dwarfs \(185\)](#)

1. Introduction

Planets form in dusty disks surrounding newly born stars. The most straightforward way to identify the presence of circumstellar disks is through infrared imaging, probing for the excess emission from warm dust. The material in the disk is a remnant from the rotating cloud core out of which the star formed, flattened into a disk-shaped structure during the collapse, as angular momentum is conserved. In star-forming regions with ages of 1–2 Myr, more than half of all GKM stars harbor disks. In somewhat older regions with ages of 5–10 Myr the disk fraction declines to 10%–20%, as the disk material is either accreted onto the stars, blown away by winds, or incorporated into planetary systems (Jayawardhana et al. 1999; Haisch et al. 2001; Meyer et al. 2007).

Disks are not only found around stars, but also for young brown dwarfs, substellar objects with masses below $0.08 M_{\odot}$, or $80 M_{\text{Jup}}$, and thus unable to sustain stable hydrogen burning. Initial discoveries and studies of such circum-substellar disks started about two decades ago (Natta et al. 2002; Jayawardhana et al. 2003; Mohanty et al. 2004), giving rise to the now well-established fact that most brown dwarfs form like stars from the collapse of cloud cores (Luhman 2012). The Spitzer Space Telescope with its unprecedented sensitivity at 3–24 μm was instrumental in furthering our understanding of brown dwarf disks. With growing samples, it became clear that brown dwarf disks are common and long lived. The disk fractions among brown dwarfs in young star-forming regions are comparable to

those of coeval stars, translating into similar disk lifetimes (Scholz & Jayawardhana 2008; Luhman & Mamajek 2012). Using Spitzer, we also learned that brown dwarf disks show evidence for the growth of dust grains (Apai et al. 2005) and dust settling to the midplane (Scholz et al. 2007)—prerequisites for planet formation via core accretion. Indeed, subsequent work at longer wavelengths, in particular with the Atacama Large Millimeter/submillimeter Array (ALMA), has shown the potential for planet formation in brown dwarf disks (Testi et al. 2016). The discovery of several planetary-mass companions orbiting brown dwarfs suggests that substellar objects with masses of 1%–8% the mass of the Sun can form their own planetary systems (Jung et al. 2018).

In parallel to the exploration of substellar disks, deep ground-based observing programs have established that star-forming regions host objects with masses that are an order of magnitude below the hydrogen burning limit. In all regions studied to sufficient depth—such as σ Orionis, ρ Ophiuchi, NGC 1333, IC348, Chamaeleon-I, Taurus, Lupus, and Upper Scorpius—surveys find objects with masses below the deuterium-burning limit of $\sim 15 M_{\text{Jup}}$ down to masses as low as $\sim 5 M_{\text{Jup}}$ (e.g., Zapatero Osorio et al. 2000; Lucas et al. 2001; Scholz et al. 2012; Lodieu et al. 2018; Miret-Roig et al. 2022).

We know very little about the nature and evolution of these free-floating planetary-mass objects (PMOs). One basic question relates to their origin: they could be formed either like stars and brown dwarfs, from the collapse of cloud cores (Bate 2012). They could also be giant planets that got ejected from their natal systems (Parker & Quanz 2012; van Elteren et al. 2019). From purely theoretical arguments, we expect a mix of formation scenarios in the 1–15 M_{Jup} mass domain, with a star-like origin more likely at the upper end of the mass range,



Original content from this work may be used under the terms of the [Creative Commons Attribution 4.0 licence](#). Any further distribution of this work must maintain attribution to the author(s) and the title of the work, journal citation and DOI.

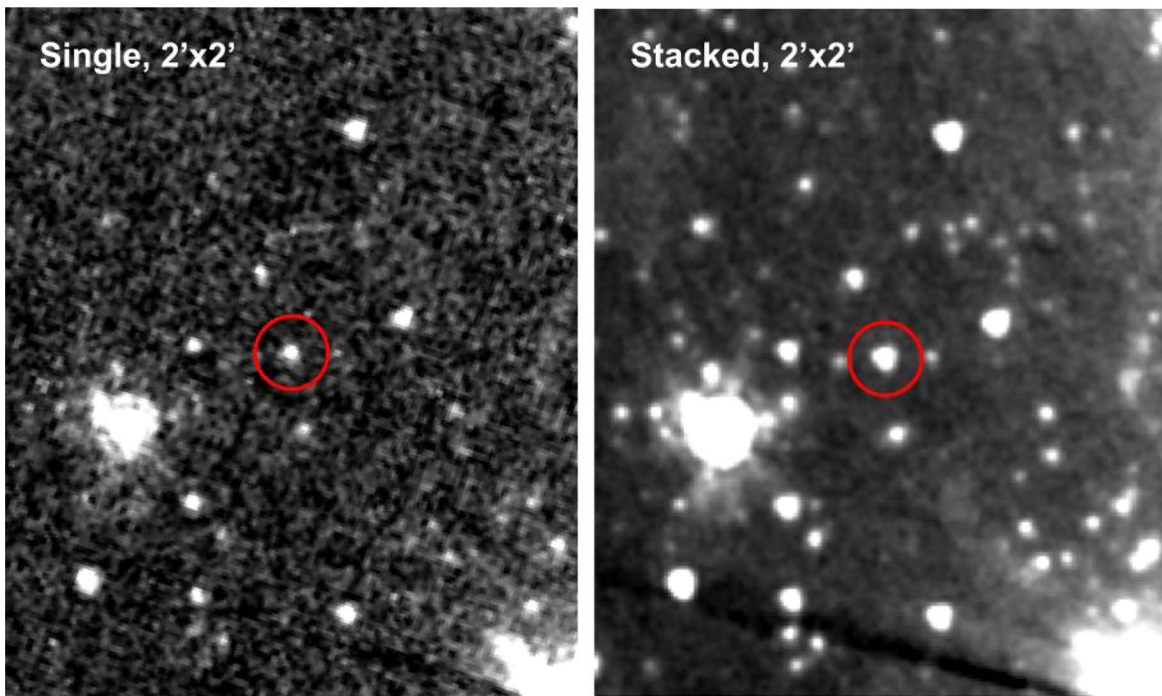


Figure 1. Comparison of a single epoch Spitzer/IRAC image of NGC 1333 in channel 2 ($4.5 \mu\text{m}$, AOR 29324032) and the stacked version of the same area (70 frames). The marked object in the center is the L3 brown dwarf SONYC-NGC1333-36, one of the lowest-mass spectroscopically confirmed objects in this cluster. The image size is $2' \times 2'$, north is up and east is left.

and a planetary origin dominant at the lower (Scholz et al. 2022). The low-mass limit for star formation, set by the opacity limit of fragmentation, is expected to be in that mass range, as well (Bate 2012). But these notions have not been verified empirically yet. Another fundamental question is whether or not these PMOs can form their own miniature planetary systems.⁶

Searching for the signature of disks around free-floating PMOs will shed light on these questions. If PMOs frequently host disks, they have at least the potential to form their own planetary systems. Follow-up studies can then clarify to what extent the prerequisites for planet formation (grain growth, sufficient dust mass, longevity) are met. If free-floating PMOs form predominantly like planets in disks around stars, we would expect their primordial disks to be disrupted (Bowler et al. 2011). Thus, at face value, we do not expect substantial disks to be common around PMOs if they themselves form in circumstellar disks. Since we expect ejected planets to become more common with decreasing mass, an important benchmark is to determine the mass below which disks become rare or nonexistent.

In this paper we present new measurements of the infrared magnitudes of PMOs in the young cluster NGC 1333, a compact active star-forming region with an age of ~ 1 Myr (Gutermuth et al. 2008; Scholz et al. 2009) and a distance of 300 pc, according to Gaia DR2 parallaxes of its member stars (Pavlidou 2022). In contrast to previous infrared surveys in this cluster, we construct new, ultra-deep Spitzer images by stacking a time-series observation. In Section 2 we present the methodology and the sample. In Section 3 we derive the infrared excess, verify the presence of disks in PMOs, and

discuss PMO disks in general. We present conclusions in Section 4.

2. Data Analysis

2.1. Image Stacking

NGC 1333 was observed as part of the YSOVAR program during Spitzer’s Warm Mission, under program id 61026. The field was observed in IRAC channels 1 ($3.6 \mu\text{m}$) and 2 ($4.5 \mu\text{m}$), in the following called IRAC1 and IRAC2. For full information on YSOVAR, see Rebull et al. (2014). In short, YSOVAR was a large-scale monitoring program with Spitzer to study variability in young stars, focused in particular on inner disk structure, accretion changes, eclipsing binaries, and rotation periods. The program surveyed 12 star-forming regions. The number of epochs varies from region to region, from a minimum of about a dozen to several thousand. NGC 1333 was one of the target regions for YSOVAR, with a survey area of 2×2 IRAC field of views, where a $10' \times 10'$ field was covered by both channels. For more information on the variability analysis of the NGC 1333 data set, see Rebull et al. (2015). The fundamental reference for the IRAC instrument is Fazio et al. (2004).

We downloaded 70 images from the YSOVAR data set on NGC 1333, for each of the two channels, from the Spitzer Heritage Archive. The images for a given channel all have very similar pointings, with minimal field rotation, and similar depth. However, due to the layout of the Spitzer focal plane, the images for channel 1 are offset compared to channel 2. Stacking was performed using the Python `reproject` package (Robitaille et al. 2020), with the function `reproject_and_coadd`. We stacked in two iterations, for each filter separately: first we created seven stacks from 10 images each, then we stacked the resulting seven stacks to a final deep image for each band. In Figure 1 we show a comparison for a

⁶ We continue to call the potential satellites of PMOs “planets,” keeping in mind that if they exist, they would not be orbiting a star, but an object itself comparable to giant planets in mass and size.

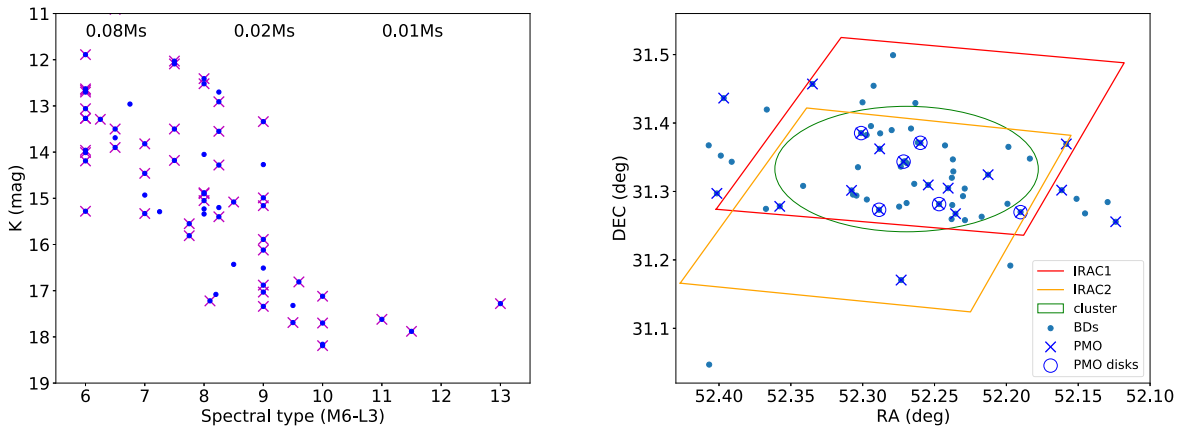


Figure 2. Left: spectral type vs. K -band magnitude for brown dwarfs in NGC 1333. The dots mark all objects in this spectral type range from the list by Luhman et al. (2016). The crosses mark the ones covered by our deep coadded Spitzer images. The spectral types are numerically coded, where M6 is 6.0, L0 is 10.0. Right: spatial distribution of brown dwarfs (small dots), PMOs (crosses), and PMOs with disks (empty circles) in NGC 1333. We also show the position and extent of the cluster as determined by Gutermuth et al. (2008), as well as approximate coverage of the deep IRAC images produced here.

part of the stacked image versus the same part of a single image.

2.2. Sample Selection

We created a catalog of brown dwarfs in NGC 1333 based on the recent census by Luhman et al. (2016), which builds on several previous surveys and includes a comprehensive literature review. Their published list comprises 203 new members, the clear majority of which are in the area covered by our deep Spitzer images. Most members have optical or near-infrared spectroscopic confirmation, either by the authors of that census, or from the literature. In addition, the authors use their own astrometry, as well as indicators of youth (e.g., X-ray emission, infrared excess) to identify cluster members. The Luhman census is “nearly complete” down to K magnitudes of 16.2 and an A_J of 3.

From that list, we selected the 65 for which the spectral type adopted by Luhman et al. (2016) is M6 or later. A spectral type of M6 is commonly used as the boundary between stars and brown dwarfs in star-forming regions. It translates to a temperature of ~ 3000 K (Mužić et al. 2014), corresponding to an object with a mass at or slightly above the substellar limit of $0.08 M_{\odot}$ for an age of 1–5 Myr, according to evolutionary tracks (Baraffe et al. 2015). That means our sample should safely encompass all known brown dwarfs in the NGC 1333 census, but may include some very-low-mass stars as well. The sample also includes 19 objects with a spectral type of M9 or later, i.e., with estimated masses near or below the deuterium-burning limit. Those PMOs are the main focus of this paper.

Of the 65 likely brown dwarfs, 49—including 14 PMOs—are covered by at least one of our deep Spitzer/IRAC images. After the Luhman et al. (2016) census, two more papers confirmed new substellar members for NGC 1333: Eskin & Luhman (2017) and Allers & Liu (2020). The former includes two more objects with M9 or later spectral type, one of which is covered by our images, and was originally reported by Oasa et al. (2008). We added it to our sample (with spectral type M9–L4, we adopt L1.5 here). Thus our total sample of PMOs is comprised of 15 objects. Due to the spatial offsets between the images in the two Spitzer/IRAC channels, a few objects in our sample are only covered by one channel. A dozen of the sources are in areas with a highly variable background or very close to the edge. Of the 65 likely brown dwarfs, 34 are in the

JKS catalog published by Scholz et al. (2012), which combines the deep J - and K -band photometry from Scholz et al. (2009) with the list of young stellar objects created from the the single-epoch Spitzer/IRAC images taken by the C2D project (Evans et al. 2009). For the objects covered by our deep Spitzer images, 23 (IRAC1) and 22 (IRAC2) are in the JKS catalog.

We characterize our sample in Figure 2. In the left panel, we show spectral type versus K -band magnitude for the whole brown dwarf catalog, marking those covered by our deep images, and indicating approximate mass limits. As can be appreciated from this figure, our sample covers the entire substellar range, from the limit between stars and brown dwarfs to masses well below the deuterium-burning limit. In particular, it includes all objects with spectral types L0 or later found in this cluster thus far. In the right panel, we plot the spatial distributions of the brown dwarfs and PMOs (marking those with disks; see Section 3). The figure demonstrates that our images cover the embedded cluster as well as the surrounding areas.

2.3. Photometry

We carried out aperture photometry for the objects in our catalog using tools from `photutils` (Bradley et al. 2021). We chose a constant aperture with a radius of 5 pixels. We note that the native pixel size of IRAC is $1''.2$, but the mosaics used here have $0''.6$ per pixel. The FWHM of IRAC during the Warm Mission is $2''.0$, according to the IRAC Instrument Handbook. An aperture radius of 5 pixels corresponds to an aperture diameter of $6''$, or approximately 3 times the FWHM, and should capture $>90\%$ of the flux. For local background estimates, we measured the median flux in an annulus with an inner and outer radius of 7 and 10 pixels, respectively, centered on the object coordinates.

The magnitudes were calibrated by direct comparison with the JKS catalog mentioned above. The offset between the JKS IRAC magnitudes, which originally come from the C2D source list (Evans et al. 2009), and our instrumental measurements is constant for a wide range of magnitudes, with standard errors of 0.03 and 0.04 mag (depending on the channel). Thus, simply adding an offset shifts our instrumental magnitudes into the standard system and makes them comparable with the literature.

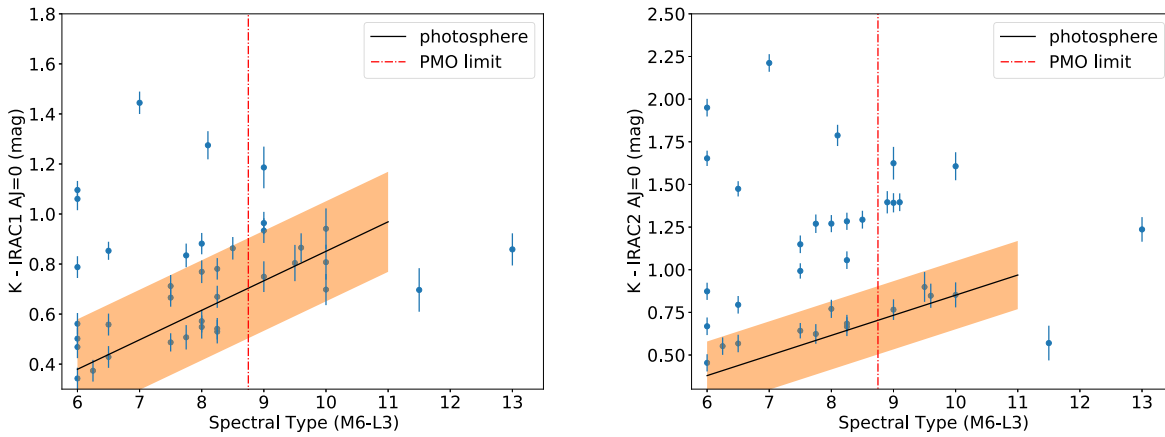


Figure 3. Infrared colors of brown dwarfs in NGC 1333 vs. spectral types, after dereddening the colors to $A_J = 0$. The spectral type range is M6–L3. In the right panel, three objects of spectral type M9 have very similar colors and have been plotted slightly offset in spectral type for clarity. The estimated photospheric colors are shown with a solid black line, with the typical scatter shown as the colored area (see the text for details). The dashed–dotted line is the chosen demarcation for our sample; all objects plotted on the right side of it can be described as PMOs.

Photometric errors were estimated by adding in quadrature the Poissonian errors in the source flux, the standard error for the background times the number of pixels in the aperture, and the error in the calibration. The median error, which is dominated by the calibration uncertainty, is 0.04 mag for both channels.

All sources were checked in the stacked images. In particular, we verified that the background determined by the photometry routine is adequate and that the aperture is well centered on the source. As indicated earlier, some objects are located in areas of highly variable background, which may affect the photometry.

Finally, we calculate the $K - \text{IRAC1}$ and $K - \text{IRAC2}$ colors using the K -band values listed in Luhman et al. (2016). We dereddened these colors to zero extinction using the published A_J extinction values for the sample, again from Luhman et al. (2016). Those values have been determined by comparing the optical and near-infrared colors to the expected photospheric values. For a subset of our sample, Scholz et al. (2012) determined extinctions, using photometry and spectroscopy. Comparing with the Luhman values, there is good agreement, with a typical uncertainty < 0.5 mag in A_J .

For the extinction correction, we convert from A_J to A_K using a standard extinction law ($A_K = 0.382 A_J$; Mathis 1990). For the IRAC wavelengths, we adopt $A_{\text{IRAC1}} = 0.6 A_K$ and $A_{\text{IRAC2}} = 0.5 A_K$. These extinction relations are in line with recently published work for star-forming regions; see Chapman et al. (2009). With very few exceptions, the brown dwarfs in our sample have an A_J below 5. Thus, the exact choice of the extinction law within plausible values does not change the outcomes in any significant way. The dereddened colors versus spectral types are plotted in Figure 3, as a way to identify objects with infrared excess emission and thus disks. These figures are the foundation for the discussion in Section 3.

For completeness, we also did full-field photometry using the SExtractor (Bertin & Arnouts 1996) for the stacked image and an individual image in both channels. Comparing the peak of the histogram for the magnitudes, we find that the stacked images are deeper by 2.4 and 2.6 mag, for IRAC1 and IRAC2, respectively. This result confirms the face-value expectation—stacking 70 images of similar quality should result in $\sqrt{70} = 8.3$ better signal-to-noise ratio, or 2.3 mag greater depth.

3. Results and Discussion

3.1. Photospheric Colours

To determine which objects have excess emission in their infrared colors we first need to establish the photospheric levels in the same colors, as a function of spectral type. We prepared a sample of stars and brown dwarfs with spectral types from M0 to L1, all without disks (and thus without infrared excess), that are members of nearby star-forming regions (< 10 Myr). In this exercise, we are building on the work in Almendros-Abad et al. (2022). The $K - \text{IRAC1}$ and $K - \text{IRAC2}$ colors for this sample show a gradual increase from values of 0.1 for early M dwarfs to around 1.0 for early L dwarfs. We fit these colors for spectral types M6 or later with a linear slope, which describes the trend seen in the data well:

$$K - \text{IRAC1} = 0.1007 \times \text{SpT} - 0.2847 \quad (1)$$

$$K - \text{IRAC2} = 0.1179 \times \text{SpT} - 0.3281 \quad (2)$$

Here, the spectral type (SpT) is 6.0 for M6 and 11.0 for L1. We tested these relations by doing the same procedure on only a subset of the diskless objects, and do not find a significant change. In particular, we limited the fit for objects with ages < 5 Myr and the fit remains very similar. For reference, the given relations are consistent with the ones published by Luhman (2022) for ages < 20 Myr.

Our photospheric colors are plotted in Figure 3 as solid lines. We also show in the figure the typical scatter of diskless objects around this fit, as the colored area. Objects without infrared excess in NGC 1333 are expected to be found in that area around the solid line in Figure 3.

3.2. Infrared Excess and Disk Fraction

In Table 1 we list the newly derived infrared photometry and colors (before extinction correction) for the 15 PMOs (spectral types M9 or later): 14 have measurements in IRAC1, 13 in IRAC2. Three objects with reported magnitudes are in areas of highly variable background, and after careful examination we deem those measurements to be unreliable. As can be seen in Figure 3, eight objects with good measurements have a dereddened $K - \text{IRAC1}$ color consistent with photospheres,

Table 1
Infrared Photometry for PMOs in NGC 1333

No	R.A. (deg)	Decl. (deg)	SpT ^a	IRAC1	IRAC2	$K - \text{IRAC1}$	$K - \text{IRAC2}$	IR ^a	Disk ^b	First Spectrum
1	52.15829	31.36939	L0	16.72		0.98		No	No	Luhman et al. (2016)
2	52.19013	31.26978	M9	16.24	15.58	0.79	1.45	Yes	Yes	Luhman et al. (2016)
3	52.21271	31.32450	M9.5	16.84	16.74	0.85	0.95	No	No	Luhman et al. (2016)
4	52.23542	31.26753	M9.6	15.94	15.96	0.87	0.85	No	No	Scholz et al. (2009)
5	52.24050	31.30478	L1.5	16.73	16.74	1.15	1.14		No	Esplin & Luhman (2017)
6	52.24683	31.28153	M9	15.02	14.52	1.10	1.60	Yes	Yes	Luhman et al. (2016)
7	52.25438	31.30956	L0	16.29	16.11	0.83	1.01	No	No	Luhman et al. (2016)
8	52.25983	31.37108	M9	15.69	15.26	1.19	1.62	Yes	Yes	Luhman et al. (2016)
9	52.27154	31.34361	M9	11.64	10.77			Yes	Yes?	Luhman et al. (2016)
10	52.27321	31.17053	M9		15.12		0.77	No	No	Scholz et al. (2009)
11	52.28817	31.36233	M9	10.84	10.65			No	No?	Luhman et al. (2016)
12	52.28858	31.27322	L0	17.21	16.53	0.98	1.66		Yes	Luhman et al. (2016)
13	52.30108	31.38531	M9	13.77	13.23	1.39	1.93	Yes	Yes	Luhman et al. (2016)
14	52.30775	31.30158	L1	17.43					No?	Scholz et al. (2012)
15	52.35771	31.27828	L3	16.42	16.04	0.86	1.24	No	No	Scholz et al. (2012)

Notes. Errors in the IRAC magnitudes are 0.03–0.09 mag.

^a Previous classification of infrared excess, from Luhman et al. (2016).

^b Our classification, based on Figure 3.

six do in $K - \text{IRAC2}$. Altogether seven sources out of 12 with robust measurements in at least one band show no evidence for infrared excess.

The remaining five objects are found to have infrared excess and are thus likely to be PMOs with disks. Four of these are at spectral type M9, three of them with excess in both bands (one with marginal excess in IRAC1). The fifth, with spectral type L0, has no excess in IRAC1, but a clear excess in IRAC2. Thus, the disk fraction from our sample is 5/12 or 42%. Due to the small sample size, the plausible range for the disk fraction is 26–60% (assuming 1σ binomial confidence intervals). Visual examination of the three objects in areas with highly variable background shows that one (SONYC-NGC1333-9) is bright in both IRAC bands, and thus also a good candidate for harboring a disk. The other two are faint and more likely to lack excess. Including those three would bring the disk fraction to 6/15, or 40%. We note that with one exception all disks in the PMO regime are found for brown dwarfs classified as M9, at the adopted upper limit for our PMO sample. For L0 or later objects, the disk fraction is only 1/5 or 20%, 1/6 if we add the one with background-affected measurements.

Our analysis includes the lowest-mass objects identified thus far in this cluster, in particular, the six objects with spectral type L0 or later (corresponding to masses of $\sim 0.01 M_{\odot}$ or lower). We determine the infrared excess for five out of six objects, with the one exception mentioned above. It is likely that the current optical/near-infrared surveys are not complete for those spectral types. Therefore, the disk fractions determined here may be affected by incompleteness at the lowest masses. If disk-bearing objects are on average deeper embedded than those without, thus having more extinction and are fainter, it is conceivable that we are underestimating the disk fraction for $M < 0.01 M_{\odot}$. This, in addition to small number statistics, may contribute to the low fraction of disks in the L0 or later domain. Deeper observations will be needed to clarify this.

In Figure 2, right panel, we show the spatial distribution of the PMOs and PMOs with disks relative to the cluster extent and the overall brown dwarf sample. There is no obvious spatial bias in those samples, they are all concentrated on the

cluster itself. One of the disk-bearing PMOs is located just outside the nominal cluster extent, but the same is true for several PMOs without disks.

Among the brown dwarfs with valid measurements and spectral types M6 to $< \text{M9}$ in our images, 8/27 show clear infrared excess in IRAC1, 15/23 in IRAC2. This corresponds to a disk fraction of $30\% \pm 10\%$ for IRAC1 and $65\% \pm 12\%$ for IRAC2. Thus, based on our measurements, the disk fraction among PMOs is consistent within the statistical uncertainties with the value for more massive brown dwarfs. We only quote these numbers for completeness: in contrast to the faint PMOs, our deep images do not provide a significant benefit for the brighter M6 to $< \text{M9}$ objects.

3.3. Comparison with the Literature

In Table 1 we also included the previous classification of the infrared excess based on Luhman et al. (2016), in the column labeled “IR”. This previous paper uses mid-infrared excess measured from Spitzer images to identify circumstellar disks. Of our list of 15, 12 have that information listed in Luhman et al. (2016), and for all 12 our classification is in agreement with the one in the literature. We also classify three objects for the first time here. One of them likely has a disk: at spectral type L0, it is currently the latest type object with a disk in NGC 1333. We also classify the three objects with spectral types later than L0 as diskless, two of them for the first time.

Luhman et al. (2016) also derived disk fractions for subsamples divided by spectral type. They report 11/21 or 52% for spectral types later than M8 (a slightly different subset than our sample of PMOs), 20/33 or 61% for M6–M8, 28/48 or 58% for M3.75–M5.75 and 27/39 or 69% for K6 to M3.5. Within the statistical error bars, these values are all consistent with each other, and with our own measurements of the disk fractions, given above. Our measurement is also consistent with the disk fraction of $66\% \pm 8\%$ for objects with spectral type of M5–M9 in NGC 1333, reported by Scholz et al. (2012). For completeness, for a sample of 79 Gaia-selected low-mass stars in NGC 1333, Pavlidou (2022) measure a disk fraction of $67\% \pm 13\%$ (for the mass range 0.1 to $1.0 M_{\odot}$, approximately).

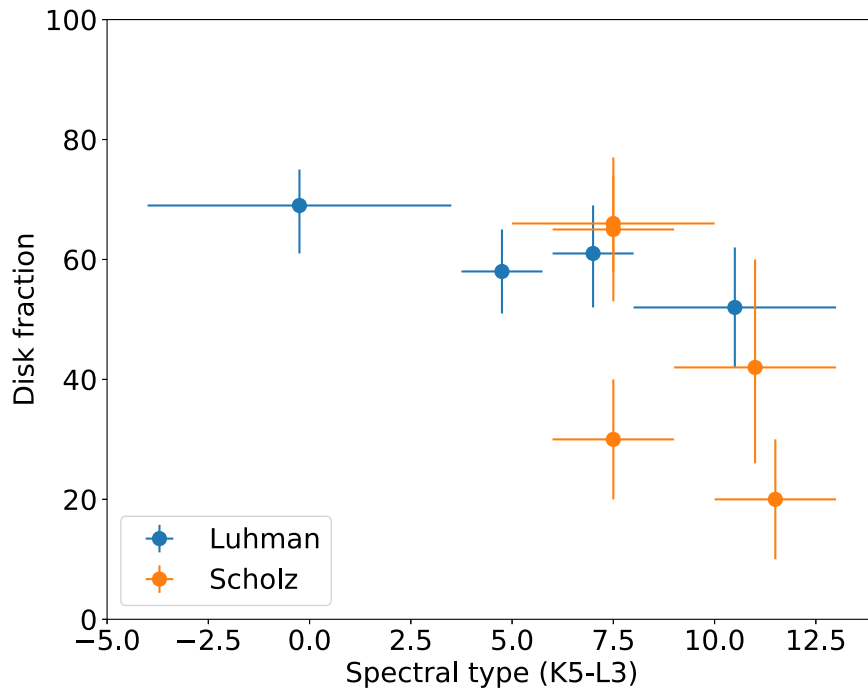


Figure 4. Disk fraction for samples of stars and brown dwarfs with known spectral type, from Luhman et al. (2016) (blue symbols), Scholz et al. (2012), and this paper (orange symbols). The spectral types are numerically coded, M0 is 0.0, L0 is 10.0.

We note here that the “disk fraction” in the quoted papers and in our study is defined as the number of Class II objects, divided over the sum of Class II and Class III. These numbers are all based on samples from optical/near-infrared surveys, and should not be compared directly with the higher disk fractions derived from mid-infrared surveys (Jørgensen et al. 2006; Gutermuth et al. 2008). One further caveat: disk surveys based on photometry at 3–8 μm can by their nature not find disks with large inner holes where the disk only causes excess emission at longer wavelengths. All studies mentioned above share this bias.

In Figure 4 we provide a summary of the currently available disk fraction measurements for low-mass stars, brown dwarfs, and PMOs in NGC 1333, including only objects with known spectral type. As can be appreciated from this figure, there is no significant trend in the disk fraction from late K to early L spectral type. In that regard, our new photometry confirms results from previous studies of the disk population for this cluster. Finding a disk fraction largely independent of mass for low-mass stars and brown dwarfs is also in line with what has been found for other star-forming regions with ages between 1 and 5 Myr, including IC348 (Luhman et al. 2016), σ Orionis (Scholz & Jayawardhana 2008), and Chamaeleon-I (Luhman et al. 2008). As a sidenote, the brown dwarf disk fraction derived in the current paper from IRAC1 excess (30%) seems to be an underestimate compared with the literature and should be treated with caution.

Figure 4 also illustrates that there may be a decline in the disk fraction when comparing L-type PMOs to K–M stars and brown dwarfs. As noted above, among the six cluster members in NGC 1333 with spectral type L0 or later only one seems to have a disk, based on our measurements, translating to a disk fraction of 20%. Given the small sample size and possible bias, as mentioned above, it is premature to conclude that this is indeed a drop-off in the disk fraction. If confirmed, it would constitute a very curious result, with possible implications for

the formation process. Finding more L-type objects in this cluster would immediately give us a better handle on this issue.

We note that for somewhat older star-forming regions, like Upper Scorpius and the TW Hydrae Association, with ages \sim 8–10 Myr, there is some evidence in the literature for an increased disk fraction for brown dwarfs compared to low-mass stars (Riaz & Gizis 2008; Luhman & Mamajek 2012; Cook et al. 2017). For those regions, PMOs do not seem to stand out from more massive brown dwarfs in terms of their disk fraction—but the small sample size hampers a more definitive assessment of the longevity of disks around PMOs.

Generally speaking, the evidence is strong that free-floating PMOs can harbour disks, and therefore, have the potential to form their own (miniature) planetary systems. In terms of the overall mass and scale, these systems would be more comparable to Jupiter’s Galilean moons than to the solar system.

3.4. The Lowest-mass Free-floating Objects with Disks

Our work in NGC 1333 reported in this paper establishes that at least five PMOs in NGC 1333 show evidence for the presence of a circum-substellar disk. The lowest mass among these is an object at spectral type L0 (not previously identified as disk bearing), corresponding to a temperature of 2200 K, which for an age of 1–2 Myr would result in an estimated mass of \sim 0.01 M_{\odot} (Baraffe et al. 2015). The three confirmed sources with later spectral types, and thus presumably lower masses, do not have detectable infrared excess and are classified as diskless.

Similar studies have been carried out in other star-forming regions. Taken together, there is now a small sample of young PMOs with securely identified disks. This includes OTS44 (Joergens et al. 2013), the only one with an ALMA detection at far-infrared/submillimeter wavelengths (Bayo et al. 2017). For young PMOs, definitively detecting an infrared excess due to a

disk is challenging work, for two reasons. One, as can be appreciated from Figure 3, the photospheric near-/mid-infrared colors increase steadily for young late M and L dwarfs. With the typical uncertainties in the spectral typing of at least ± 1 subtype, the photospheric level for a given source is uncertain. Second, these are faint sources, and thus, the near-/mid-infrared magnitudes come with considerable errors. Both difficulties worsen toward later spectral types and lower masses. They can be overcome with deeper mid-infrared images (the motivation for this study), improved spectroscopic classification, or photometry at wavelengths where the photospheric flux is negligible compared to the disk excess (10 μm or beyond).

With all that in mind, we summarize the results for regions with sufficient survey depth.

In σ Orionis, two planetary-mass brown dwarfs (SOri 60 and SOri 71) have consistently been found to host disks at wavelengths up to 8 μm (Luhman et al. 2008; Scholz & Jayawardhana 2008). These two have spectral types of L2 and L0, respectively. This cluster is slightly older than NGC 1333; for its age of 3–5 Myr, these spectral types would correspond to $\sim 0.01 M_{\odot}$ or above. There are some PMOs with later spectral types and claimed excess emission (e.g., SOri 65, 66, and 70), but the mid-infrared data are inconclusive (Luhman et al. 2008; Scholz & Jayawardhana 2008). In the case of SOri 70, it is also not clear yet if it is in fact a young member of the cluster and not a foreground brown dwarf (Zapatero Osorio et al. 2017).

In Chamaeleon-I, OTS44 (M9.5) is a secure detection. In addition, Luhman et al. (2008) found Cha 1107–7626, an L0 object with a disk. Esplin et al. (2017) report three more objects with M9–L2/L3 spectral types that may have excess emission, but caution against interpreting it as evidence for a disk. Given the uncertainty in their spectral type, more work needs to be done before assigning masses or infrared excess to those.

In Taurus, the lowest-mass objects with safely detected disks have late M spectral types, according to the recent survey by Esplin & Luhman (2019). Some L0–L1 sources also may have infrared excess. In addition, Esplin & Luhman (2019) find one very-low-mass source with an L3 spectral type, which would have a mass well below $0.01 M_{\odot}$, with possible excess emission at 4.5 μm . Again, this is not a robust detection yet.

ρ Ophiuchi has spectroscopically confirmed brown dwarfs with disks at spectral type M9–L1 (Testi et al. 2002; Jayawardhana & Ivanov 2006; Alves de Oliveira et al. 2012), which again would correspond to a mass of $\sim 0.01 M_{\odot}$. CFHTWIR-Oph-33 has a spectral type of L3–L4 and may have excess emission, but the mid-infrared data are inconclusive in that regard (Alves de Oliveira et al. 2012; Esplin & Luhman 2020). Some other very-low-mass objects discussed in these papers may have infrared excess, but also very uncertain spectral type (e.g., CFHTWIR-Oph-58, with a range from M8.5 to L3; see Almendros-Abad et al. 2022).

Finally, the older Upper Scorpius association has a large population of brown dwarfs. Two with a spectral type of L3.5 are reported to have accretion and infrared excess (Lodieu et al. 2018). For ages of 5–10 Myr, this would correspond to $0.01 M_{\odot}$ or above. To our knowledge, no lower-mass objects with disks have been found here.

In summary, at this stage, the low-mass limit for objects with a *safe* disk detection, across all star-forming regions, is $\sim 0.01 M_{\odot}$ (or $\sim 10 M_{\text{Jup}}$). The surveys have found perhaps two dozen objects in total that may have masses below that

limit (depending on how the mass is estimated) in all of the very young regions mentioned above. For the majority of them we can already firmly rule out the presence of disks—the lowest-mass objects in NGC 1333 discussed in this paper belong in that category. For about ten of these PMOs with putative masses $< 0.01 M_{\odot}$, the currently available data are inconclusive and insufficient for proper characterization. Therefore, it is certainly too early to rule out the presence of disks around objects with masses below $0.01 M_{\odot}$. Having said that, given that the disk fraction among brown dwarfs is 30%–60% for the young regions mentioned above, the lack of confirmed disks below the $0.01 M_{\odot}$ limit is perhaps already worth noting, especially if taken together with our new measurements for NGC 1333, as illustrated in Figure 4. If the disk fraction were similar for objects with masses $< 0.01 M_{\odot}$, essentially all objects with tentative detections of infrared excess should have disks. Perhaps we are beginning to see a decline of disk fractions in the planetary-mass domain.

Sensitive mid-infrared observations of known PMOs, and deep surveys for new objects in this mass domain are needed to verify this suspicion. JWST is primed to help with both of these tasks. In NGC 1333 specifically, a Guaranteed Time program with NIRISS/WFSS is dedicated to a deep spectroscopic survey, and designed to find PMOs in this cluster down to masses of $1 M_{\text{Jup}}$ (program ID 1202; see Willott et al. 2022). Also, the unprecedented sensitivity of the MIRI instrument will enable us to probe directly for infrared excess in the lowest-mass free-floating objects known, at wavelengths exceeding those of Spitzer/IRAC, allowing for unambiguous disk detections.

The presence of disks is discussed in the literature as one possible signature to distinguish between a star-like and a planet-like formation scenario (Luhman 2012; Testi et al. 2016). In particular, if an object gets ejected early in the evolution from a forming planetary system, either by planet–planet scattering or encounters with other stars, it can be expected that its disk, if present, will be affected. Simulations on this issue, however, remain sparse or nonexistent. For the case of planet–planet-scattering, Bowler et al. (2011) demonstrate that the disruption of a circumplanetary disk should be common. In this context, disks detected with ALMA around young giant planets on wide orbits are an interesting comparison. These planetary-mass companions may have very compact disks (Wu et al. 2017), but it is unclear whether or not their masses are lower than expected from the standard relation between disk mass and stellar mass (Wu et al. 2020).⁷

Given the discussed arguments, it is plausible to assume that free-floating planets that have been ejected from a young planetary system would not host massive, long-lasting disks. If future observations confirm the absence of disks for objects with masses below $0.01 M_{\odot}$, it may indicate that this is the low-mass limit for objects to form like stars, physically set by the opacity limit for fragmentation.

4. Summary




We present new Spitzer/IRAC photometry of brown dwarfs with planetary masses in the young star-forming cluster NGC 1333. To improve on previous findings, we stack 70

⁷ In the simulations by Stamatellos & Herczeg (2015) objects that formed in disks around stars are found to harbour their own disks with substantial masses, but the authors do not model the effect an ejection might have on those disks.

images taken as a time-series campaign during Spitzer’s Warm Mission in 2011, at wavelengths of 3.6 and 4.5 μm . Our deep images cover 50 brown dwarfs, 15 of which have spectral types of M9 or later, corresponding to masses near or below the deuterium-burning limit (i.e., PMOs). Out of 12 PMOs with good measurements, five show clear infrared emission in excess of the estimated photospheric level. Taken together with previous work, our results confirm that the disk fraction does not change significantly between very-low-mass stars, brown dwarfs, and PMOs. Thus, free-floating objects with masses comparable to those of giant planets have the potential to form their own miniature planetary systems. However, we note that among the six lowest-mass objects in NGC 1333, with spectral types of L0 or later, only one has a clear disk detection (no. 12 in Table 1), which may be a sign of a drop-off in disk fraction at ultralow masses, possibly suggesting that objects at these masses are primarily ejected planets, rather than formed from core collapse. We survey the literature for studies on disks around PMOs and find that the lowest-mass objects with a firmly detected disks have masses around $0.01 M_{\odot}$. Some objects at later spectral types have tentative detections of infrared excess, but whether or not this is significant and due to the presence of a disk is still uncertain. Future observations with JWST will undoubtedly probe the presence of disks around lower-mass objects, thus shedding light on the formation mechanism of free-floating PMOs.

We thank the anonymous referee for a constructive and concise referee report on this paper. This work is based on observations made with the Spitzer Space Telescope, which was operated by the Jet Propulsion Laboratory, California Institute of Technology under a contract with NASA. V.A. and K.M. acknowledge funding by the Science and Technology Foundation of Portugal (FCT), grants Nos. PTDC/FIS-AST/7002/2020, UIDB/00099/2020, and SFRH/BD/143433/2019. Constructive discussions with Dimitris Stamatellos, Ken Rice, Ian Bonnell, and James Wurster have aided the discussion in this paper.

ORCID iDs

Aleks Scholz  <https://orcid.org/0000-0001-8993-5053>
 Koraljka Muzic  <https://orcid.org/0000-0002-7989-2595>
 Ray Jayawardhana  <https://orcid.org/0000-0001-5349-6853>

References

- Allers, K. N., & Liu, M. C. 2020, *PASP*, 132, 104401
 Almendros-Abad, V., Mužić, K., Moitinho, A., et al. 2022, *A&A*, 657, A129
 Alves de Oliveira, C., Moraux, E., Bouvier, J., et al. 2012, *A&A*, 539, A151
 Apai, D., Pascucci, I., Bouwman, J., et al. 2005, *Sci*, 310, 834
 Baraffe, I., Homeier, D., Allard, F., et al. 2015, *A&A*, 577, A42
 Bate, M. R. 2012, *MNRAS*, 419, 3115
 Bayo, A., Joergens, V., Liu, Y., et al. 2017, *ApJL*, 841, L11
 Bertin, E., & Arnouts, S. 1996, *A&AS*, 117, 393
 Bowler, B. P., Liu, M. C., Kraus, A. L., et al. 2011, *ApJ*, 743, 148
 Bradley, L., Sipőcz, B., Robitaille, T., et al. 2021, *astropy/photutils*: 1.3.0, Zenodo, doi:10.5281/zenodo.5796924
 Chapman, N. L., Mundy, L. G., Lai, S.-P., et al. 2009, *ApJ*, 690, 496
 Cook, N. J., Scholz, A., & Jayawardhana, R. 2017, *AJ*, 154, 256
 Esplin, T. L., & Luhman, K. L. 2017, *AJ*, 154, 134
 Esplin, T. L., & Luhman, K. L. 2019, *AJ*, 158, 54
 Esplin, T. L., & Luhman, K. L. 2020, *AJ*, 159, 282
 Esplin, T. L., Luhman, K. L., Faherty, J. K., et al. 2017, *AJ*, 154, 46
 Evans, N. J., Dunham, M. M., Jørgensen, J. K., et al. 2009, *ApJS*, 181, 321
 Fazio, G. G., Hora, J. L., Allen, L. E., et al. 2004, *ApJS*, 154, 10
 Gutermuth, R. A., Myers, P. C., Megeath, S. T., et al. 2008, *ApJ*, 674, 336
 Haisch, K. E., Lada, E. A., & Lada, C. J. 2001, *ApJL*, 553, L153
 Jayawardhana, R., Ardila, D. R., Stelzer, B., et al. 2003, *AJ*, 126, 1515
 Jayawardhana, R., Hartmann, L., Fazio, G., et al. 1999, *ApJL*, 521, L129
 Jayawardhana, R., & Ivanov, V. D. 2006, *ApJL*, 647, L167
 Joergens, V., Bonnefoy, M., Liu, Y., et al. 2013, *A&A*, 558, L7
 Jørgensen, J. K., Harvey, P. M., Evans, N. J., et al. 2006, *ApJ*, 645, 1246
 Jung, Y. K., Udalski, A., Gould, A., et al. 2018, *AJ*, 155, 219
 Lodieu, N., Zapatero Osorio, M. R., Béjar, V. J. S., et al. 2018, *MNRAS*, 473, 2020
 Lucas, P. W., Roche, P. F., Allard, F., et al. 2001, *MNRAS*, 326, 695
 Luhman, K. L. 2012, *ARA&A*, 50, 65
 Luhman, K. L. 2022, *AJ*, 163, 24
 Luhman, K. L., Allen, L. E., Allen, P. R., et al. 2008, *ApJ*, 675, 1375
 Luhman, K. L., Esplin, T. L., & Loutrel, N. P. 2016, *ApJ*, 827, 52
 Luhman, K. L., Hernández, J., Downes, J. J., et al. 2008, *ApJ*, 688, 362
 Luhman, K. L., & Mamajek, E. E. 2012, *ApJ*, 758, 31
 Mathis, J. S. 1990, *ARA&A*, 28, 37
 Meyer, M. R., Backman, D. E., Weinberger, A. J., et al. 2007, in *Protostars and Planets V*, ed. B. Reipurth, D. Jewitt, & K. Keil (Tucson, AZ: Univ. Arizona Press), 573
 Miret-Roig, N., Bouy, H., Raymond, S. N., et al. 2022, *NatAs*, 6, 89
 Mohanty, S., Jayawardhana, R., Natta, A., et al. 2004, *ApJ*, 609, L33
 Mužić, K., Scholz, A., Geers, V. C., et al. 2014, *ApJ*, 785, 159
 Natta, A., Testi, L., Comerón, F., et al. 2002, *A&A*, 393, 597
 Oasa, Y., Tamura, M., Sunada, K., et al. 2008, *AJ*, 136, 1372
 Parker, R. J., & Quanz, S. P. 2012, *MNRAS*, 419, 2448
 Pavlidou, T. 2022, PhD Thesis, Univ. St Andrews
 Rebull, L. M., Cody, A. M., Covey, K. R., et al. 2014, *AJ*, 148, 92
 Rebull, L. M., Stauffer, J. R., Cody, A. M., et al. 2015, *AJ*, 150, 175
 Riaz, B., & Gizis, J. E. 2008, *ApJ*, 681, 1584
 Robitaille, T., Deil, C., & Ginsburg, A. 2020, reproject: Python-based astronomical image reprojection, Astrophysics Source Code Library, ascl:2011.023
 Scholz, A., Geers, V., Jayawardhana, R., et al. 2009, *ApJ*, 702, 805
 Scholz, A., & Jayawardhana, R. 2008, *ApJL*, 672, L49
 Scholz, A., Jayawardhana, R., Muzic, K., et al. 2012, *ApJ*, 756, 24
 Scholz, A., Jayawardhana, R., Wood, K., et al. 2007, *ApJ*, 660, 1517
 Scholz, A., Muzic, K., Geers, V., et al. 2012, *ApJ*, 744, 6
 Scholz, A., Muzic, K., Jayawardhana, R., et al. 2022, *PASP*, 134, 104401
 Stamatellos, D., & Herczeg, G. J. 2015, *MNRAS*, 449, 3432
 Testi, L., Natta, A., Oliva, E., et al. 2002, *ApJL*, 571, L155
 Testi, L., Natta, A., Scholz, A., et al. 2016, *A&A*, 593, A111
 van Elteren, A., Portegies Zwart, S., Pelupessy, I., et al. 2019, *A&A*, 624, A120
 Willott, C. J., Doyon, R., Albert, L., et al. 2022, *PASP*, 134, 025002
 Wu, Y.-L., Bowler, B. P., Sheehan, P. D., et al. 2020, *AJ*, 159, 229
 Wu, Y.-L., Close, L. M., Eisner, J. A., et al. 2017, *AJ*, 154, 234
 Zapatero Osorio, M. R., Béjar, V. J. S., Martín, E. L., et al. 2000, *Sci*, 290, 103
 Zapatero Osorio, M. R., Béjar, V. J. S., & Peña Ramírez, K. 2017, *ApJ*, 842, 65